
Counterfactual Maps: What They Are and How to Find Them

Awa Khouna¹ Julien Ferry¹ Thibaut Vidal¹

Abstract

Counterfactual explanations are a central tool in interpretable machine learning, yet computing them exactly for complex models remains challenging. For tree ensembles, predictions are piecewise constant over a large collection of axis-aligned hyperrectangles, implying that an optimal counterfactual for a point corresponds to its projection onto the nearest rectangle with an alternative label under a chosen metric. Existing methods largely overlook this geometric structure, relying either on heuristics with no optimality guarantees or on mixed-integer programming formulations that do not scale to interactive use. In this work, we revisit counterfactual generation through the lens of nearest-region search and introduce *counterfactual maps*, a global representation of recourse for tree ensembles. Leveraging the fact that any tree ensemble can be compressed into an equivalent partition of labeled hyperrectangles, we cast counterfactual search as the problem of identifying the *generalized Voronoi cell* associated with the nearest rectangle of an alternative label. This leads to an exact, amortized algorithm based on volumetric k-dimensional (KD) trees, which performs branch-and-bound nearest-region queries with explicit optimality certificates and sublinear average query time after a one-time preprocessing phase. Our experimental analyses on several real datasets drawn from high-stakes application domains show that this approach delivers globally optimal counterfactual explanations with millisecond-level latency, achieving query times that are orders of magnitude faster than existing exact, cold-start optimization methods.

1. Introduction

Counterfactual explanations have become a cornerstone of interpretable machine learning, providing actionable insights by identifying how an input must change to alter a model’s prediction. Their appeal spans regulated domains such as credit scoring, healthcare, and criminal justice, where explanations must be both meaningful and reliable. Despite this importance, generating *optimal* counterfactual explanations remains a major challenge for complex models, particularly tree ensembles.

Tree ensembles, including random forests and gradient boosted trees, are among the most widely used models for tabular data. They achieve strong predictive performance while offering some interpretability through feature-based splits. Geometrically, these models partition the input space into a collection of axis-aligned hyperrectangles, each with a constant prediction. A globally optimal counterfactual for a given input is therefore the point of minimum distance within any hyperrectangle with an alternative label.

Most existing approaches treat counterfactual generation as a *per-instance* optimization problem. Heuristic approaches (Tolomei et al., 2017; Carreira-Perpinan & Hada, 2023; Mothilal et al., 2020) traverse decision paths within trees or perturb inputs to find label-changing points, but provide no guarantees of optimality. In practice, these methods may converge to poor local minima, overshoot the minimal required changes, or fail to return a feasible counterfactual even when one exists, exposing *some* of the end users to explanations that may be invalid or unnecessarily costly (Parmentier & Vidal, 2021). Exact methods instead rely on mixed-integer programming or satisfiability formulations (Parmentier & Vidal, 2021; Karimi et al., 2020), which provide global optimality certificates at the cost of scalability: solving a mathematical program for each query quickly becomes prohibitive for large ensembles or interactive use. Consequently, no approach simultaneously offers global optimality and low query latency for realistic tree ensembles.

In this work, we argue that this limitation arises from focusing on individual counterfactuals rather than exploiting the *global structure* of counterfactual explanations through preprocessing. We introduce *counterfactual maps*: global representations that associate each point in the feature space with its nearest decision region of an alternative label, as

¹CIRRELT & SCALE-AI Chair in Data-Driven Supply Chains, Department of Mathematics and Industrial Engineering, Polytechnique Montréal, Canada. Correspondence to: Thibaut Vidal <thibaut.vidal@edu.polymtl.ca>.

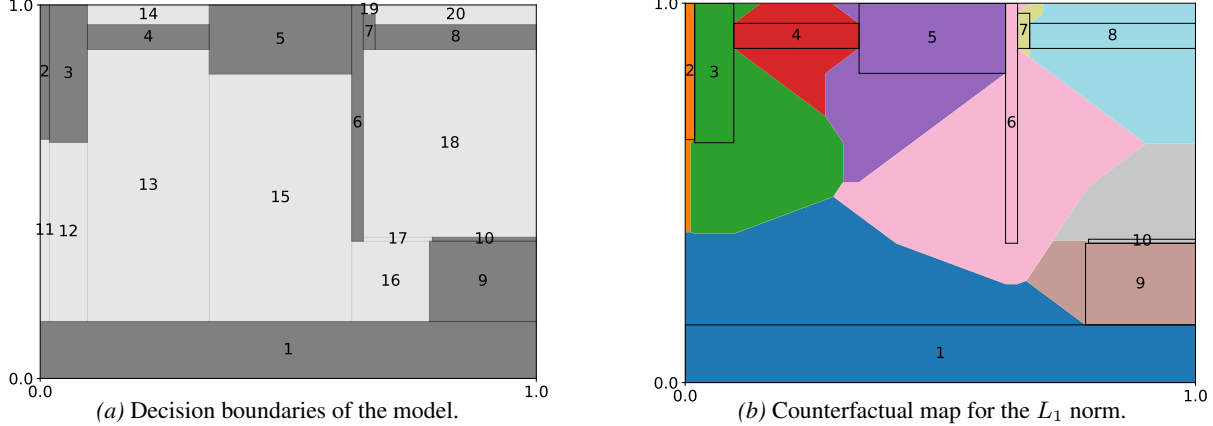


Figure 1. Counterfactual map for target class y_2 . The map corresponds to the *generalized Voronoi partition* induced by the hyperrectangles of this class. For any input query, it identifies the closest hyperrectangle of this class; projecting the query onto that region yields a globally optimal counterfactual. This simple example uses a random forest with two depth-5 trees trained on the “blobs” dataset.

illustrated in Figure 1. Such maps enable direct access to globally optimal counterfactuals at query time without requiring the solution of a new optimization problem.

A key observation underlying counterfactual maps is that any tree ensemble admits an equivalent representation as a decision tree partitioning the feature space into labeled hyperrectangles (Vidal & Schiffer, 2020). Under this representation, counterfactual generation reduces to a nearest-region problem. The feature space can therefore be partitioned into *generalized Voronoi cells* induced by these hyperrectangles, where each cell identifies the region yielding the closest counterfactual. Counterfactual maps can be viewed as implicit representations of this Voronoi decomposition.

Building on this perspective, we develop methods to efficiently construct and query counterfactual maps using a two-stage preprocess-and-query paradigm. In a one-time preprocessing step, we extract a labeled hyperrectangular partition equivalent to the ensemble’s decision function and index it using geometric search structures. At query time, this index identifies the nearest opposing region and produces a globally optimal counterfactual by projection. We instantiate this framework using orthogonal range searching and volumetric KD-trees, which provide explicit optimality certificates and achieve sublinear average query time. Our experiments on synthetic and real-world tabular datasets demonstrate that counterfactual maps enable globally optimal counterfactual explanations with interactive latency, yielding fast, guaranteed, and scalable counterfactual explanations for tree ensembles.

2. Counterfactual Maps

We consider classifiers of the form $\mathcal{T} : \mathcal{X} \rightarrow \mathcal{Y}$, where the input domain is a product space $\mathcal{X} = \mathcal{X}_1 \times \dots \times \mathcal{X}_m$, with

mixed continuous, categorical, and binary features, and the output space consists of c classes, $\mathcal{Y} = \{y_1, \dots, y_c\}$.

Tree ensembles and induced partitions. A tree ensemble (random forest, gradient-boosted trees) induces a piecewise-constant decision function. Each decision tree partitions \mathcal{X} into hyperrectangles associated with leaf predictions. Aggregating all trees yields a finite collection of *regions* over which the ensemble prediction is constant. These regions can be represented as a finite set of disjoint axis-aligned hyperrectangles (Vidal & Schiffer, 2020):

$$\mathbb{H} \triangleq \{\mathcal{H}_1, \dots, \mathcal{H}_n\}, \quad \bigcup_{i=1}^n \mathcal{H}_i = \mathcal{X}, \quad \mathcal{H}_i \cap \mathcal{H}_j = \emptyset \quad \forall i \neq j.$$

Each region \mathcal{H}_i is associated with a unique class label $\mathcal{T}(\mathcal{H}_i)$. In the worst case, the number of regions n grows exponentially with the depth of the ensemble.

Optimal counterfactuals. Let $d_p(\cdot, \cdot)$ denote an L_p distance on \mathcal{X} . For any point $x \in \mathcal{X}$ and hyperrectangle $\mathcal{H} \subseteq \mathcal{X}$, we define the point–rectangle distance

$$d_p(x, \mathcal{H}) \triangleq \inf_{x' \in \mathcal{H}} \|x - x'\|_p,$$

which admits a closed-form, coordinate-wise expression for all $p \geq 1$. Let $\Pi_{\mathcal{H}}(x)$ denote a projection of x onto \mathcal{H} attaining this minimum. More generally, we allow feature-wise weights $w \in \mathbb{R}_+^m$ to reflect different actionability costs and use the weighted norm $\|u\|_{p,w} \triangleq \|\text{diag}(w)u\|_p$, equivalently rescaling coordinates by $\tilde{x} = \text{diag}(w)x$. For readability, we write d_p and understand it as either the standard or weighted L_p distance.

For an input x with prediction $y = \mathcal{T}(x)$ and a target label $y' \neq y$, define the set of regions with label y'

$$\mathbb{H}_{y'} \triangleq \{\mathcal{H} \in \mathbb{H} \mid \mathcal{T}(\mathcal{H}) = y'\}.$$

A globally optimal counterfactual targeting y' is obtained by projecting x onto any minimizer

$$\mathcal{H}^* \in \arg \min_{\mathcal{H} \in \mathbb{H}_{y'}} d_p(x, \mathcal{H}), \quad x_{\text{cf}} \triangleq \Pi_{\mathcal{H}^*}(x).$$

Definition 2.1 (Counterfactual map). Given a tree ensemble \mathcal{T} inducing a partition \mathbb{H} of the feature space, a distance d_p , and a target label y' , a *counterfactual map* is a mapping $\hat{f}_{y'} : \mathcal{X} \rightarrow \mathbb{H}_{y'}$ such that, for every $x \in \mathcal{X}$,

$$\hat{f}_{y'}(x) \in \arg \min_{\mathcal{H} \in \mathbb{H}_{y'}} d_p(x, \mathcal{H}).$$

The associated counterfactual explanation is then obtained by projection: $x_{\text{cf}} = \Pi_{\hat{f}_{y'}(x)}(x)$. Note that the minimizer in Definition 2.1 may not be unique (notably for $p \in \{1, \infty\}$). Any selection from the argmin set yields a globally optimal counterfactual via projection.

Problem statement. Given a tree ensemble \mathcal{T} , a distance d_p , and a target label y' , our objective is to construct a counterfactual map (or an equivalent data structure) that, for any query point x , identifies the nearest region of class y' . Subsequently, the counterfactual is obtained by projecting onto this region. This paper focuses on efficiently constructing and querying such counterfactual maps.

Structural properties. Counterfactual maps admit a geometric interpretation as generalized Voronoi diagrams of the feature space induced by the hyperrectangles in $\mathbb{H}_{y'}$. The geometry of the resulting cells depends on the choice of the distance d_p , as formalized below.

Proposition 2.2. For $p \in [1, \infty]$ and $\mathcal{H}_i \in \mathbb{H}_{y'}$, define the (closed) p -Voronoi region $\mathcal{V}_i^{(p)} \triangleq \{x \in \mathcal{X} : d_p(x, \mathcal{H}_i) \leq d_p(x, \mathcal{H}_j) \forall \mathcal{H}_j \in \mathbb{H}_{y'}\}$, and for $\mathcal{H}_i, \mathcal{H}_j \in \mathbb{H}_{y'}$ the bisector $B_{ij}^{(p)} \triangleq \{x \in \mathcal{X} : d_p(x, \mathcal{H}_i) = d_p(x, \mathcal{H}_j)\}$.

• For $p \in \{1, \infty\}$ and any $\mathcal{H}_i, \mathcal{H}_j \in \mathbb{H}_{y'}$, the bisector $B_{ij}^{(p)}$ is a finite union of polyhedra. Consequently, each region $\mathcal{V}_i^{(p)}$ is a finite union of polyhedra.

• For $p = 2$ and any $\mathcal{H}_i, \mathcal{H}_j \in \mathbb{H}_{y'}$, the bisector $B_{ij}^{(2)}$ is contained in a finite union of quadratic hypersurfaces; in particular, Voronoi regions are not polyhedral in general.

A proof of Proposition 2.2 is given in Appendix A. Figure 7 in Appendix B illustrates the different counterfactual map boundaries under the L_1 , L_2 and L_∞ norms. Given the observed nonlinearities in general cases, we opted to represent counterfactual maps implicitly via certified nearest-region search rather than explicitly constructing the Voronoi decomposition. Notably, the KD-tree branch-and-bound procedure introduced in Section 3 applies generally to any L_p distance.

3. Methodology

We introduce a two-stage preprocess-and-query pipeline, illustrated in Figure 2. The preprocessing stage is executed

once per model and constructs the counterfactual maps, i.e., geometric indices over the ensemble decision regions, one for each possible target class. Subsequently, the query stage uses the appropriate map to answer targeted counterfactual requests with low latency by locating and projecting onto the nearest region of the desired class.

3.1. Constructing the Counterfactual Map

Constructing a counterfactual map requires a geometric representation of the ensemble’s decision function that is both *complete*, i.e., covering the entire feature space, and *faithful*, in the sense that it preserves the original class assignment on every region. Violations of either property would lead to counterfactual explanations that are incorrect or suboptimal.

Any tree ensemble admits such a representation as a partition of the feature space into disjoint, labeled axis-aligned hyperrectangles, as defined in Section 2. While a naïve construction could be obtained by intersecting all split thresholds across the ensemble (giving an intractable, exponentially large partition), we rely instead on the born-again tree framework of Vidal & Schiffer (2020) as an extraction mechanism, since it produces a compact region-based representation that is globally faithful to the ensemble’s predictions, i.e., it encodes the same decision function. That work proposes two algorithms: a dynamic programming approach that yields a minimal partition in terms of the number of hyperrectangles, at the cost of substantial computational and memory overhead; and a faster heuristic procedure that preserves faithfulness while relaxing minimality. As minimality has only a moderate impact on query-time complexity, we rely on the latter to limit preprocessing cost.

The resulting labeled hyperrectangles are then indexed to form the counterfactual maps. For each target class y' , we build a separate volumetric KD-tree over the subset $\mathbb{H}_{y'}$, yielding a hierarchical spatial index that supports efficient nearest-region queries. This preprocessing is performed once per model and amortized across all subsequent counterfactual queries, in contrast to exact counterfactual methods based on mixed-integer programming, which solve a global optimization problem for each query. Algorithm 1 summarizes the preprocessing pipeline.

Algorithm 1 Preprocessing the Counterfactual Maps

Input: Trained tree ensemble \mathcal{T}

Output: One KD-tree per target class y'

- 1: Extract the rectangular partition \mathbb{H} from \mathcal{T} using the heuristic of Vidal & Schiffer (2020)
- 2: For each $\mathcal{H}_i \in \mathbb{H}$, store its bounds and class label
- 3: **for** each class $y' \in \mathcal{Y}$ **do**
- 4: Build a volumetric KD-tree over $\mathbb{H}_{y'}$, storing at each node a bounding box enclosing its rectangles
- 5: **end for**

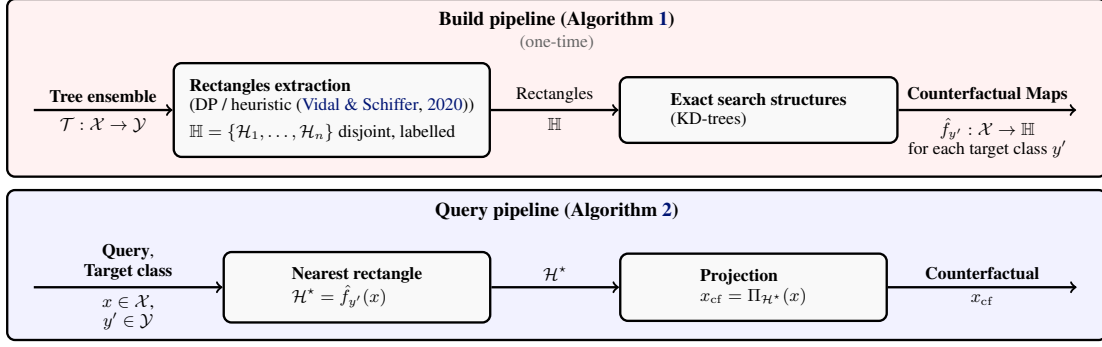


Figure 2. Two-stage workflow for counterfactual generation in tree-ensemble decision spaces. The *Build pipeline* (one-time) extracts the labeled rectangular partition \mathbb{H} and constructs an exact counterfactual map using geometric search structures. The *Query pipeline* identifies the nearest opposing region and projects the query to produce a globally optimal counterfactual explanation.

3.2. Indexing the Map for Dynamic Queries

Once constructed, the counterfactual maps act as geometric oracles to support exact nearest-region queries. Given a query point x and a target label y' , the task is to identify the region in $\mathbb{H}_{y'}$ minimizing the point-rectangle distance d_p , and to return the corresponding counterfactual by projection.

A naive evaluation of all regions in $\mathbb{H}_{y'}$ would require linear time in the size of the partition and is therefore impractical. Instead, we perform certified nearest-region search using a branch-and-bound traversal of the KD-tree associated with the target class y' . This procedure relies on admissible lower bounds on the distance from the query point to all hyperrectangles contained in a subtree, allowing entire subtrees to be pruned without sacrificing optimality. In practice, this yields sublinear average query time, as only a small fraction of nodes is typically visited.

Algorithm 2 details the query procedure. The algorithm maintains a priority queue of KD-tree nodes ordered by their lower bounds. At each iteration, the node with the smallest bound is explored; the search terminates as soon as this bound exceeds the best distance found so far. When a leaf node is reached, distances to the contained hyperrectangles of class y' are evaluated explicitly, and the current best solution is updated accordingly. Once the nearest target region \mathcal{H}^* is identified, the counterfactual explanation is obtained by projection, $x_{cf} = \Pi_{\mathcal{H}^*}(x)$. The following result formalizes the correctness of the query procedure.

Theorem 3.1 (Exact Nearest-Hyperrectangle Search). *Let $\mathbb{H}_{y'}$ be the set of axis-aligned hyperrectangles associated with a target label y' , and let d_p be an L_p distance with $1 \leq p \leq \infty$. Given a query point $x \in \mathbb{R}^m$, Algorithm 2 returns a hyperrectangle*

$$\mathcal{H}^* \in \arg \min_{\mathcal{H} \in \mathbb{H}_{y'}} d_p(x, \mathcal{H}),$$

and the projection $x_{cf} = \Pi_{\mathcal{H}^}(x)$ is a globally optimal counterfactual explanation targeting class y' under d_p .*

A detailed proof of Theorem 3.1 is provided in Appendix C. It relies on the fact that the branch-and-bound traversal maintains valid lower bounds on the distance to all unexplored regions, ensuring that no region that could improve the current best solution is ever pruned. Termination occurs only when no unexplored subtree can contain a closer target region, guaranteeing global optimality.

Algorithm 2 Exact Counterfactual Query (Targeted)

Input: Query point x , KD-tree over $\mathbb{H}_{y'}$, distance d_p
Output: Optimal counterfactual x_{cf}

- 1: Initialize best distance & region $(d^*, \mathcal{H}^*) \leftarrow (\infty, \text{null})$
- 2: Initialize a min-priority queue Q with the root node of the KD-tree for class y'
- 3: **while** Q is not empty **do**
- 4: Pop a node v from Q (with smallest lower bound $d_p(x, B(v))$)
- 5: **if** $d_p(x, B(v)) \geq d^*$ **then**
- 6: **break**
- 7: **end if**
- 8: **if** v is a leaf **then**
- 9: **for** each $\mathcal{H} \in \mathbb{H}_{y'}(v)$ **do**
- 10: Compute $d \leftarrow d_p(x, \mathcal{H})$
- 11: **if** $d < d^*$ **then**
- 12: $(d^*, \mathcal{H}^*) \leftarrow (d, \mathcal{H})$
- 13: **end if**
- 14: **end for**
- 15: **else**
- 16: **for** each child c of v **do**
- 17: **if** $d_p(x, B(c)) < d^*$ **then**
- 18: Insert c into Q
- 19: **end if**
- 20: **end for**
- 21: **end if**
- 22: **end while**
- 23: $x_{cf} \leftarrow \Pi_{\mathcal{H}^*}(x)$

4. Experimental Analyses

We evaluate the proposed counterfactual maps algorithm (**CF-Maps**) on a diversity of tabular classification benchmarks and compare against state-of-the-art exact and heuristic counterfactual methods for random forests. Our experiments address two main questions: (i) to what extent can preprocessing amortize the cost of exact counterfactuals to achieve interactive query latency, and (ii) how does CF-Maps compare to existing exact and heuristic baselines in terms of runtime and counterfactual quality.

4.1. Experimental setup

Datasets. We consider four datasets of significant interest in trustworthy machine learning, summarized in Table 1 and encompassing numerical, categorical, ordinal, and binary features. These datasets are linked to high-stakes tasks such as recidivism prediction (CP), credit risk assessment (FI), and medical prognosis or disease prevalence prediction (BC and PD), where system audits, explanation quality, and recourse are particularly critical. To ensure consistency and reproducibility, we follow the same preprocessing pipeline as in Vidal & Schiffer (2020) for feature scaling and encoding of categorical variables.

Table 1. Characteristics of the datasets used in our experiments: number of samples, features, and sample-class distribution

Dataset	#Samples	#Features	Classes
Breast-Cancer (BC)	683	9	65-35
COMPAS (CP)	6907	12	54-46
FICO (FI)	10459	17	52-48
Pima-Diabetes (PD)	768	8	65-35

Models. For each dataset, we train random forests using the SCIKIT-LEARN Python library (Pedregosa et al., 2011), varying the number of trees (3, 5, 7, 10, 50, or 100) and their maximum depth (3, 5, 7, or 10). We repeat all experiments over five random seeds. Each dataset is split into 80% for training and 20% for testing. For each trained forest, we generate counterfactual explanations for a total of 1000 query points, drawn uniformly from the test set and supplemented, if necessary, with uniformly sampled inputs.

Baselines. We compare the proposed **CF-Maps** against three baselines that cover both exact and heuristic counterfactual generation for random forests:

- **OCEAN** (Parmentier & Vidal, 2021) is a mixed-integer optimization method that returns globally optimal counterfactuals. We use the reference implementation `oceanpy` from PyPI¹ with its default solver settings.
- **Feature Tweaking (FT)** (Tolomei et al., 2017) is a heuris-

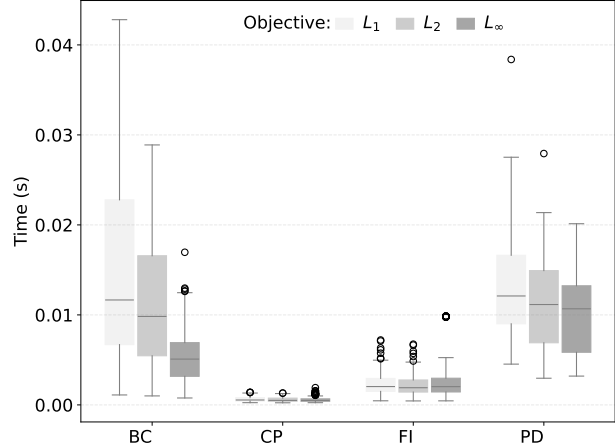


Figure 3. Average query latency of **CF-Maps** after the one-time preprocessing step (i.e., time to generate a counterfactual explanation using Algorithm 2), for three distance functions across all datasets, for random forests with 100 depth-5 trees.

tic procedure that perturbs decision paths to flip predictions. We use the public implementation from the repository `featureTweakPy`².

- **LIRE** (Carreira-Perpinan & Hada, 2023) is a heuristic method which restricts the search space to regions supported by the training data (a.k.a live regions). Since, to our knowledge, no official implementation is available, we reproduced LIRE as described in its paper.

We further discuss these baselines and position our approach with respect to related work in Section 5.

Setup. All experiments are run on a computing cluster over a set of homogeneous nodes equipped with AMD EPYC 7532 (Zen 2) @2.40GHz CPU with 64GB of RAM. All materials (source code and datasets) required to reproduce our experiments will be released publicly upon acceptance as a Python library under an MIT license.

4.2. Main Results

Result 1. CF-Maps achieves millisecond-to-subsecond query times suitable for interactive use while delivering optimal counterfactuals. Figure 3 reports the average time required by CF-Maps to generate each counterfactual explanation for a standard random forest configuration of 100 depth-5 trees, averaged over five random seeds and 1000 queries, after the one-time preprocessing step. Across datasets, CF-Maps returns optimal counterfactuals within fractions of a second, ranging from a few milliseconds on COMPAS to a few tens of milliseconds on Breast-Cancer. Variability across datasets is primarily driven by dimensionality (number of features), but also by feature type: numeri-

¹<https://pypi.org/project/oceanpy/>

²<https://github.com/upura/featureTweakPy>

Table 2. Preprocessing time (T_0) and total time (preprocessing + queries) to generate 50 and 1000 counterfactuals (T_{50} and T_{1000}), for random forests with 100 depth-5 trees, for all datasets. We also indicate the error ratio R over the 1000 counterfactuals compared to the optimum. For FT, we additionally report the proportion of queries for which no feasible counterfactual is found (%Fail).

Dataset	OCEAN				CF-Maps				LIRE				FT				
	T_0	T_{50}	T_{1000}	R	T_0	T_{50}	T_{1000}	R	T_0	T_{50}	T_{1000}	R	T_0	T_{50}	T_{1000}	%Fail	R
BC	3.3	104.2	1367.6	1.0	8.8	9.6	14.1	1.0	2.9	3.0	4.3	3.1	0.0	24.3	480.3	96.0	1.0
CP	6.4	55.8	993.4	1.0	0.3	0.3	0.9	1.0	1.4	1.5	2.3	1.3	0.0	75.2	726.6	70.2	2.0
FI	6.6	119.6	2214.6	1.0	1.6	1.8	4.2	1.0	21.4	22.0	33.6	1.2	0.0	33.3	674.5	79.9	1.9
PD	6.4	787.5	12664.0	1.0	234.4	235.1	245.8	1.0	6.0	6.1	9.7	10.2	0.0	25.3	507.0	82.1	3.3

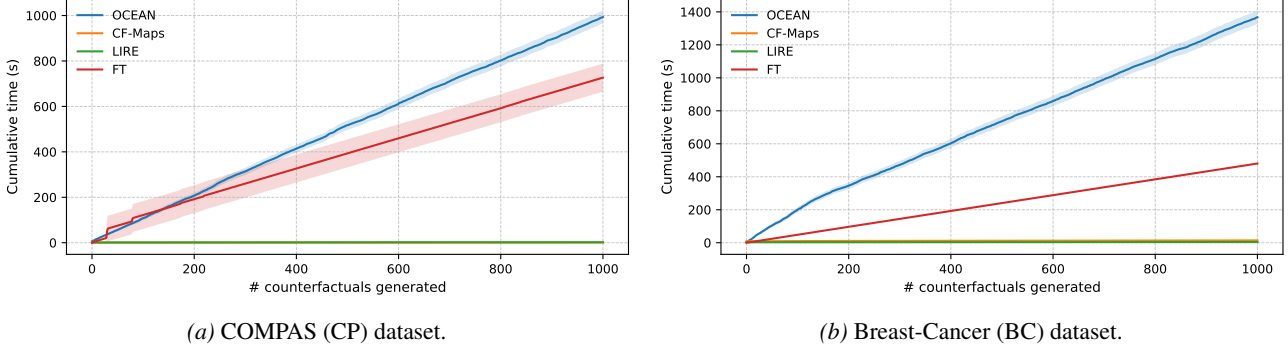


Figure 4. Total runtime (including one-time preprocessing and counterfactual generation) as a function of the number of generated counterfactuals, for random forests with 100 depth-5 trees.

cal attributes typically induce many distinct split thresholds, leading to a partition with more hyperrectangles in \mathbb{H} and a deeper volumetric KD-tree.

Result 2. CF-Maps adapts effectively to different norms. Figure 3 demonstrates that CF-Maps can efficiently handle all considered distances, namely the L_1 , L_2 , and L_∞ norms, while maintaining interactive query latency. We observe a consistent trend: query time is slightly higher under the L_1 norm and slightly lower under L_∞ , with L_2 in between. Intuitively, this behavior reflects pruning efficiency in our KD-tree branch-and-bound search: because regions are axis-aligned hyperrectangles, distance lower bounds tend to be tighter under L_∞ , leading to fewer visited nodes on average.

Result 3. CF-Maps is orders of magnitude faster than the state-of-the-art for generating optimal counterfactual explanations, while heuristic baselines are suboptimal and often slower. Table 2 compares CF-Maps with existing exact and heuristic baselines across all datasets for random forests with 100 depth-5 trees. We report preprocessing time, total time to generate 50 or 1000 counterfactuals, and the average error ratio defined as the factor by which heuristic methods overestimate the distance to the optimal counterfactual. Preprocessing includes hyperrectangle extraction and volumetric KD-tree construction (Algorithm 1) for CF-Maps, building the mixed-integer formulation for OCEAN, and extracting live regions for LIRE.

As shown in the table, heuristic methods incur substantially higher recourse costs, with error ratios reaching up to $10\times$ for LIRE and $3\times$ for FT relative to the optimum. Moreover, FT’s error ratio is computed only over queries for which a valid counterfactual is found; for the realistic-size random forests considered here, FT fails to return any feasible counterfactual for most queries (from roughly 70% on COMPAS to 96% on BC). In contrast, OCEAN consistently returns optimal counterfactuals, but its runtime grows markedly with the number of queries, as each explanation requires solving a new optimization problem.

CF-Maps avoids both limitations: it delivers globally optimal counterfactuals while achieving query latency comparable to LIRE and orders of magnitude lower than OCEAN (and often FT). Figure 4 further illustrates that the one-time preprocessing cost is amortized after only a few queries, after which CF-Maps generates optimal counterfactual explanations at very low computational cost, often faster than the considered heuristics. Figure 8 in Appendix D shows the same trends on the remaining datasets.

4.3. Sensitivity Analyses

Result 4. CF-Maps scales to larger and deeper forests while retaining optimality, whereas exact and heuristic baselines degrade in runtime or solution quality. Figure 5 reports the total time required to generate 1000 counterfactuals

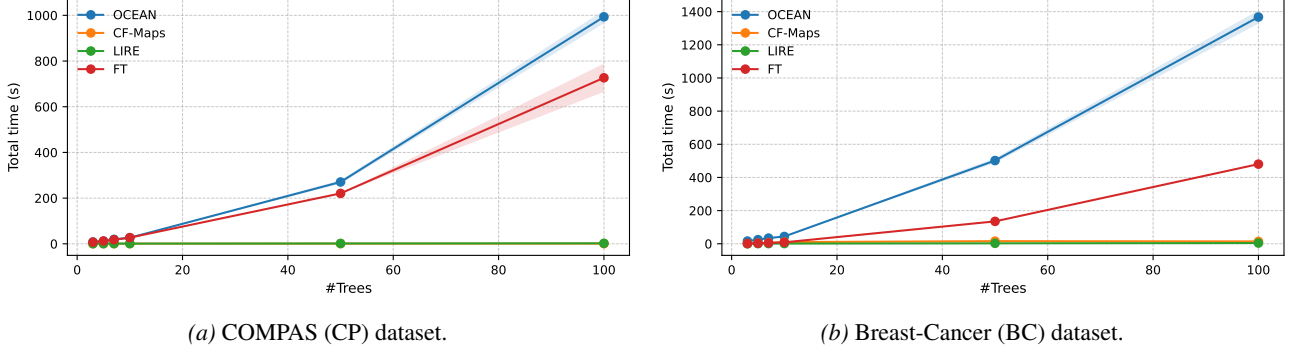


Figure 5. Total runtime (including one-time preprocessing and counterfactual generation) for generating 1000 counterfactuals, for random forests with varying numbers of depth-5 trees.

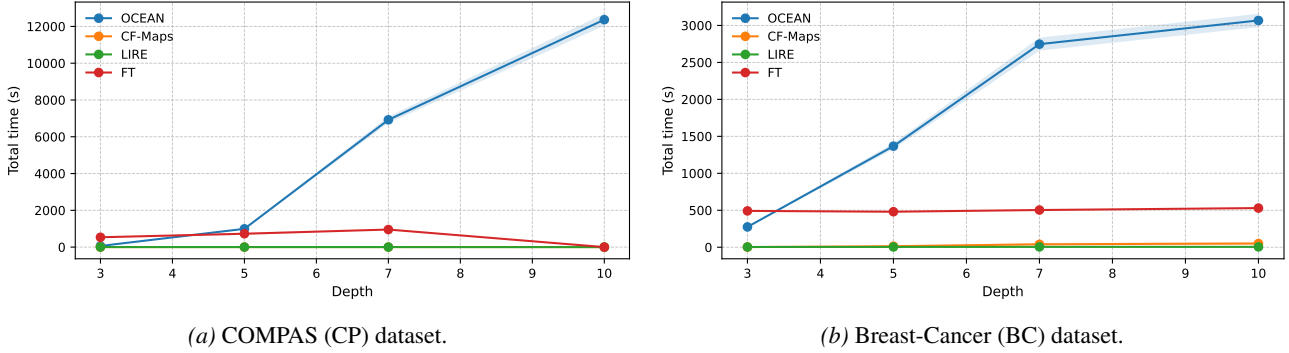


Figure 6. Total runtime (including one-time preprocessing and counterfactual generation) for generating 1000 counterfactuals, for random forests with 100 trees of varying depth.

als for random forests with an increasing number of depth-5 trees (results for the remaining datasets are provided in Figure 9 in Appendix D). As the number of trees grows, the runtimes of OCEAN and FT increase substantially, reflecting the fact that OCEAN solves a new optimization problem per query and FT evaluates an increasing number of candidate tweakings.

Figure 6 shows similar trends when varying tree depth within a random forest with 100 trees: CF-Maps consistently maintains interactive query latency, while OCEAN slows down markedly as depth increases. LIRE scales relatively well computationally, since restricting the search to live regions makes its runtime depend primarily on the training set size rather than on the ensemble size.

Table 3 in Appendix D complements these results by assessing the quality of counterfactuals produced by LIRE and FT. Overall, heuristics deteriorate as forests grow. FT increasingly fails to find any feasible counterfactual (e.g., from 22.7% failures for 3 depth-5 trees on COMPAS to roughly 70% for 100 trees), while LIRE, although always feasible by design, becomes substantially more suboptimal, with error ratios increasing from about 2× (3 trees on Pima-Diabetes) to more than 10× (100 trees).

5. Related works

Counterfactual explanations are a cornerstone of trustworthy machine learning, as they provide intuitive, instance-level explanations of model predictions. We review prior work on counterfactual explanations for tree ensembles, distinguishing between heuristic and exact methods, and then discuss amortized inference approaches. For broader surveys on counterfactual explanations, we refer the reader to Karimi et al. (2022), Guidotti (2024), and Verma et al. (2024).

While early counterfactual explanation methods were largely model-agnostic (Wachter et al., 2017), *white-box* approaches tailored to a specific hypothesis class can often produce higher-quality explanations by exploiting model structure. For tree ensembles, many existing methods generate counterfactuals *heuristically*, that is, without guarantees on optimality or even feasibility. A widely used baseline specific to tree ensembles is Feature Tweaking (FT) (Tolomei et al., 2017), which explores alternative root-to-leaf paths in individual trees to propose feature changes that may flip the ensemble’s prediction. However, because it does not reason jointly over all trees, FT can yield suboptimal explanations and may fail to find a valid counterfactual even when one exists. Other heuristic approaches include gradient-

based optimization using differentiable approximations of tree splits (Lucic et al., 2022), restricting the search to *live regions* supported by training data (Carreira-Perpinan & Hada, 2023), or approximating the ensemble with a single surrogate tree (Fernández et al., 2020). More recently, EECE (Zhang & Zhong, 2025) improves FT by prioritizing candidate modifications using the ensemble structure and combining them with live regions to ensure feasibility.

While the aforementioned methods are typically computationally efficient, they often provide explanations with unnecessarily high recourse costs, which can undermine trustworthiness. To address this limitation, several works propose *optimal* counterfactual generation for tree ensembles using mathematical programming or SAT/SMT formulations (Cui et al., 2015; Kanamori et al., 2020; Karimi et al., 2020; Parmentier & Vidal, 2021). OCEAN (Parmentier & Vidal, 2021) represents the current state of the art in this category, leveraging tight linear relaxations and flow-based encodings to compute optimal counterfactuals within seconds for moderately sized forests. Beyond mathematical programming, Blanchart (2021) builds a query-specific search tree that enumerates candidate regions nearby the query by intersecting split conditions (i.e., combinations of leaves) and applies branch-and-bound to prune them. Despite their guarantees, these exact methods require solving a new optimization problem for each query, limiting their applicability in interactive settings.

Finally, a smaller body of work investigates amortized counterfactual inference, where an upfront preprocessing phase enables fast counterfactual generation at query time. These approaches either rely on differentiable models to exploit gradient information (Mahajan et al., 2019; Van Looveren et al., 2021; Yang et al., 2021; Guo et al., 2021), or are model-agnostic and thus cannot exploit the internal structure of a given tree ensemble. The latter category includes GAN-based methods (Nemirovsky et al., 2022) as well as formulations based on Markov decision processes (Verma et al., 2022) or reinforcement learning (Samoilescu et al., 2021). In a different vein, using only black-box access, Becker et al. (2021) constructs a hierarchical partition of the input space by iteratively sampling within regions (starting from the full space), subdividing regions with inconsistent predictions, and then leveraging this hierarchy to accelerate counterfactual search at query time. Finally, Rawal & Lakkaraju (2020) precomputes a covering set of counterfactual examples that provides broad query coverage, but may be suboptimal for a given instance.

To the best of our knowledge, our method is the first to provide optimal counterfactual explanations for tree ensembles with amortized inference, by leveraging a counterfactual map representation that supports interactive use.

6. Conclusions

In this work, we have introduced the concept of *counterfactual maps*, which provide a direct, query-conditioned view of recourse. Beyond pointwise explanations, counterfactual maps constitute a form of global explanation: they make explicit the geometric organization of decision regions in the input space and enable interactive exploration of how recourse varies across queries.

To implement this approach, we proposed to rely on a one-time preprocessing step to construct a volumetric KD-tree for each target class. At query time, this data structure identifies the closest decision region of the desired class, and projecting the query onto that region directly yields an optimal counterfactual. Across extensive experimental analyses on datasets with numerical, binary, and categorical features, and under different objective functions, we observe that this approach achieves sublinear average query time (a few ms) while still providing optimal counterfactuals. In contrast, a comparison with existing heuristics and exact methods reveals that existing heuristics (FT and LIRE) substantially overshoot the minimal recourse cost (by factors up to 10) or frequently fail to find feasible counterfactuals when they exist (up to a 96% failure rate for FT), while OCEAN, which represents the current state of the art in terms of optimal counterfactual explanations, takes orders of magnitude more total time to generate 1000 explanations. Taken together, these results establish this methodology as a very promising solution for delivering trustworthy recourse in interactive, real-world deployments.

The research avenues stemming from this work are numerous. On the algorithmic side, additional refinements could permit speeding up the extraction of the tree ensemble partition at scale, which remains the dominant preprocessing bottleneck. To further decrease preprocessing effort, one could also consider constructing lower- or upper-envelope approximations of the partition, enabling approximate recourse with provable guarantees, or designing gating mechanisms that handle most queries interactively while triggering exact cold-start optimization only in rare, difficult cases. Finally, extending counterfactual maps to other hypothesis classes is a compelling research avenue. A similar methodology, grounded in volumetric KD-trees, could be applied to any model whose decision function is piecewise constant over axis-aligned regions (e.g., rule-based models, or models operating on discretized features). Extending the approach beyond this setting might also be possible, though it would likely require different geometric data structures.

Impact Statement

Counterfactual explanations provide actionable recourse by indicating how an input could change to obtain a different outcome. They are especially relevant and increasingly used in regulated, high-stakes domains such as credit and healthcare, where transparency and reason-giving obligations call for meaningful and reliable explanations (e.g., transparency requirements for high-risk systems in the EU AI Act, and adverse-action notices stating the principal reasons for denial under U.S. Regulation B, with related notice obligations under the Fair Credit Reporting Act).

Yet, computing counterfactual explanations reliably remains challenging for complex models such as tree ensembles. Fast heuristics can return unnecessarily costly recourse or fail to find recourse when it exists, while exact optimization-based methods are generally too slow for interactive use. Our work bridges this gap for random forests by introducing counterfactual maps, which shift computation to a one-time preprocessing step and enable interactive query-time access to optimal counterfactual explanations.

We expect this to support scalable deployment of trustworthy recourse and downstream uses such as model auditing, debugging, and visualization. To facilitate adoption and reproducibility, we will release an open-source Python implementation under an MIT license.

At the same time, interactive recourse tools can introduce risks, including strategic manipulation, overreliance on model outputs, or exposure of sensitive model behavior. We view counterfactual maps as a decision-support component that should be deployed with safeguards such as domain-appropriate feasibility constraints and distance metrics, monitoring, and human oversight. This is especially important in high-stakes settings or when model confidentiality or data privacy are concerns, where additional security or privacy-preserving mechanisms may be required.

References

Becker, M., Burkart, N., Birnstill, P., and Beyerer, J. A step towards global counterfactual explanations: Approximating the feature space through hierarchical division and graph search. *Adv. Artif. Intell. Mach. Learn.*, 1(2): 90–110, 2021.

Blanchart, P. An exact counterfactual-example-based approach to tree-ensemble models interpretability. *arXiv preprint arXiv:2105.14820*, 2021.

Carreira-Perpinan, M. A. and Hada, S. S. Very fast, approximate counterfactual explanations for decision forests. *Proceedings of the AAAI Conference on Artificial Intelligence*, 37(6):6935–6943, 2023.

Cui, Z., Chen, W., He, Y., and Chen, Y. Optimal action extraction for random forests and boosted trees. In *Proceedings of the 21th ACM SIGKDD international conference on knowledge discovery and data mining*, pp. 179–188, 2015.

Fernández, R. R., De Diego, I. M., Aceña, V., Fernández-Isabel, A., and Moguerza, J. M. Random forest explainability using counterfactual sets. *Information Fusion*, 63: 196–207, 2020.

Guidotti, R. Counterfactual explanations and how to find them: literature review and benchmarking. *Data Mining and Knowledge Discovery*, 38(5):2770–2824, 2024.

Guo, H., Nguyen, T., and Yadav, A. Counternet: End-to-end training of counterfactual aware predictions. In *ICML Workshop on Algorithmic Recourse*, 2021.

Kanamori, K., Takagi, T., Kobayashi, K., and Arimura, H. Dace: Distribution-aware counterfactual explanation by mixed-integer linear optimization. In *IJCAI*, pp. 2855–2862, 2020.

Karimi, A.-H., Barthe, G., Balle, B., and Valera, I. Model-agnostic counterfactual explanations for consequential decisions. In *International conference on artificial intelligence and statistics*, pp. 895–905. PMLR, 2020.

Karimi, A.-H., Barthe, G., Schölkopf, B., and Valera, I. A survey of algorithmic recourse: contrastive explanations and consequential recommendations. *ACM Computing Surveys*, 55(5):1–29, 2022.

Lucic, A., Oosterhuis, H., Haned, H., and De Rijke, M. Focus: Flexible optimizable counterfactual explanations for tree ensembles. In *Proceedings of the AAAI conference on artificial intelligence*, volume 36, pp. 5313–5322, 2022.

Mahajan, D., Tan, C., and Sharma, A. Preserving causal constraints in counterfactual explanations for machine learning classifiers. In *CausalML: Machine Learning and Causal Inference for Improved Decision Making Workshop, NeurIPS 2019*, 2019.

Mothilal, R. K., Sharma, A., and Tan, C. Explaining machine learning classifiers through diverse counterfactual explanations. In *Proceedings of the 2020 Conference on Fairness, Accountability, and Transparency, FAT* 2020*, pp. 607–617. ACM, 2020.

Nemirovsky, D., Thiebaut, N., Xu, Y., and Gupta, A. CounterGAN: Generating counterfactuals for real-time recourse and interpretability using residual gans. In *Uncertainty in Artificial Intelligence*, pp. 1488–1497. PMLR, 2022.

Parmentier, A. and Vidal, T. Optimal counterfactual explanations in tree ensembles. In *International conference on machine learning*, pp. 8422–8431. PMLR, 2021.

Pedregosa, F., Varoquaux, G., Gramfort, A., Michel, V., Thirion, B., Grisel, O., Blondel, M., Prettenhofer, P., Weiss, R., Dubourg, V., Vanderplas, J., Passos, A., Cournapeau, D., Brucher, M., Perrot, M., and Duchesnay, E. Scikit-learn: Machine learning in Python. *Journal of Machine Learning Research*, 12:2825–2830, 2011.

Rawal, K. and Lakkaraju, H. Beyond individualized recourse: Interpretable and interactive summaries of actionable recourses. *Advances in Neural Information Processing Systems*, 33:12187–12198, 2020.

Samoilescu, R.-F., Van Looveren, A., and Klaise, J. Model-agnostic and scalable counterfactual explanations via reinforcement learning. *arXiv preprint arXiv:2106.02597*, 2021.

Tolomei, G., Silvestri, F., Haines, A., and Lalmas, M. Interpretable predictions of tree-based ensembles via actionable feature tweaking. In *Proceedings of the 23rd ACM SIGKDD International Conference on Knowledge Discovery and Data Mining*, KDD ’17. ACM, 2017.

Van Looveren, A., Klaise, J., Vacanti, G., and Cobb, O. Conditional generative models for counterfactual explanations. *arXiv preprint arXiv:2101.10123*, 2021.

Verma, S., Hines, K., and Dickerson, J. P. Amortized generation of sequential algorithmic recourses for black-box models. In *Proceedings of the AAAI Conference on Artificial Intelligence*, volume 36, pp. 8512–8519, 2022.

Verma, S., Boonsanong, V., Hoang, M., Hines, K., Dickerson, J., and Shah, C. Counterfactual explanations and algorithmic recourses for machine learning: A review. *ACM Computing Surveys*, 56(12):1–42, 2024.

Vidal, T. and Schiffer, M. Born-again tree ensembles. In *International conference on machine learning*, pp. 9743–9753. PMLR, 2020.

Wachter, S., Mittelstadt, B., and Russell, C. Counterfactual explanations without opening the black box: Automated decisions and the gdpr. *Harvard Jounal of Law & Technology*, 31:841, 2017.

Yang, F., Alva, S. S., Chen, J., and Hu, X. Model-based counterfactual synthesizer for interpretation. In *Proceedings of the 27th ACM SIGKDD conference on knowledge discovery & data mining*, pp. 1964–1974, 2021.

Zhang, H. and Zhong, J. Efficient and effective counterfactual explanations for random forests. *Expert Systems with Applications*, pp. 128661, 2025.

A. Proof of Proposition 2.2

Proof. Since \mathbb{H} is finite, $\mathbb{H}_{y'} \subseteq \mathbb{H}$ is finite as well. First, we highlight a closed form for $d_p(x, \mathcal{H})$. Fix an axis-aligned hyperrectangle $\mathcal{H} = [a, b] \subseteq \mathbb{R}^m$ with $a \leq b$. For $k = 1, \dots, m$, define

$$\delta_k(x, \mathcal{H}) \triangleq \max\{0, a_k - x_k, x_k - b_k\}, \quad \delta(x, \mathcal{H}) \triangleq (\delta_1(x, \mathcal{H}), \dots, \delta_m(x, \mathcal{H})).$$

Let $\Pi_{\mathcal{H}}(x)$ be the coordinate-wise clamp of x to $[a, b]$, such that $|x_k - (\Pi_{\mathcal{H}}(x))_k| = \delta_k(x, \mathcal{H})$ for all k . For any $p \in [1, \infty]$,

$$d_p(x, \mathcal{H}) = \inf_{x' \in \mathcal{H}} \|x - x'\|_p = \|x - \Pi_{\mathcal{H}}(x)\|_p = \|\delta(x, \mathcal{H})\|_p. \quad (1)$$

Case $p \in \{1, \infty\}$. For each sign pattern $s \in \{-1, 0, +1\}^m$, consider the polyhedron

$$R_s(\mathcal{H}) \triangleq \{x : x_k \leq a_k \text{ if } s_k = -1; a_k \leq x_k \leq b_k \text{ if } s_k = 0; x_k \geq b_k \text{ if } s_k = +1\}.$$

On $R_s(\mathcal{H})$, each $\delta_k(\cdot, \mathcal{H})$ is affine. Hence, by (1),

- $d_1(\cdot, \mathcal{H}) = \sum_k \delta_k(\cdot, \mathcal{H})$ is affine on $R_s(\mathcal{H})$;
- $d_\infty(\cdot, \mathcal{H}) = \max_k \delta_k(\cdot, \mathcal{H})$ is the maximum of finitely many affine functions on $R_s(\mathcal{H})$, and is therefore affine on a finite polyhedral refinement obtained by fixing an index attaining the maximum.

Consequently, for each $\mathcal{H} \in \mathbb{H}_{y'}$ and $p \in \{1, \infty\}$, there exists a finite polyhedral partition $\mathcal{P}(\mathcal{H})$ of \mathbb{R}^m such that $d_p(\cdot, \mathcal{H})$ is affine on every cell of $\mathcal{P}(\mathcal{H})$. Let $\mathcal{P} \triangleq \bigwedge_{\mathcal{H} \in \mathbb{H}_{y'}} \mathcal{P}(\mathcal{H})$ be the common refinement, i.e., the partition whose cells are all nonempty intersections of one cell from each partition $\mathcal{P}(\mathcal{H})$ with $\mathcal{H} \in \mathbb{H}_{y'}$. \mathcal{P} is still a finite polyhedral partition, and for every $C \in \mathcal{P}$ and every $\mathcal{H} \in \mathbb{H}_{y'}$, the function $d_p(\cdot, \mathcal{H})$ is affine on C .

Fix $\mathcal{H}_i, \mathcal{H}_j \in \mathbb{H}_{y'}$. On each $C \in \mathcal{P}$, the bisector condition $d_p(x, \mathcal{H}_i) = d_p(x, \mathcal{H}_j)$ is an equality of two affine functions, hence it defines either $C \cap H$ for some hyperplane H , or all of C (when the affine functions coincide on C). Therefore

$$B_{ij}^{(p)} = \{x : d_p(x, \mathcal{H}_i) = d_p(x, \mathcal{H}_j)\}$$

is a finite union of polyhedra.

Similarly, for fixed $\mathcal{H}_i \in \mathbb{H}_{y'}$ and any $C \in \mathcal{P}$,

$$\mathcal{V}_i^{(p)} \cap C = \{x \in C : d_p(x, \mathcal{H}_i) \leq d_p(x, \mathcal{H}_j) \ \forall \mathcal{H}_j \in \mathbb{H}_{y'}\}$$

is given by finitely many linear inequalities on C , hence is a polyhedron (possibly empty). Since \mathcal{P} is finite, $\mathcal{V}_i^{(p)}$ is a finite union of polyhedra.

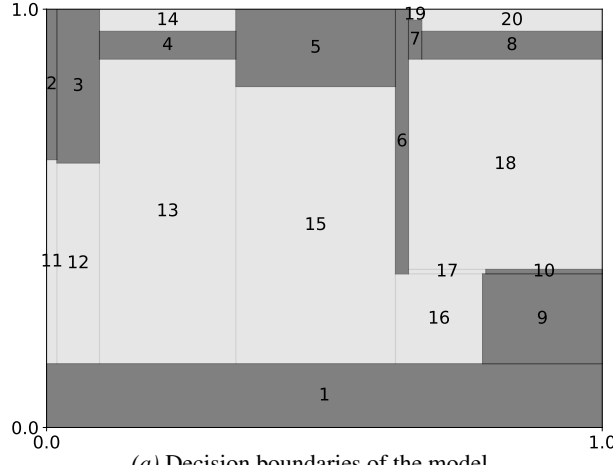
Case $p = 2$. By (1),

$$d_2(x, \mathcal{H})^2 = \sum_{k=1}^m \delta_k(x, \mathcal{H})^2.$$

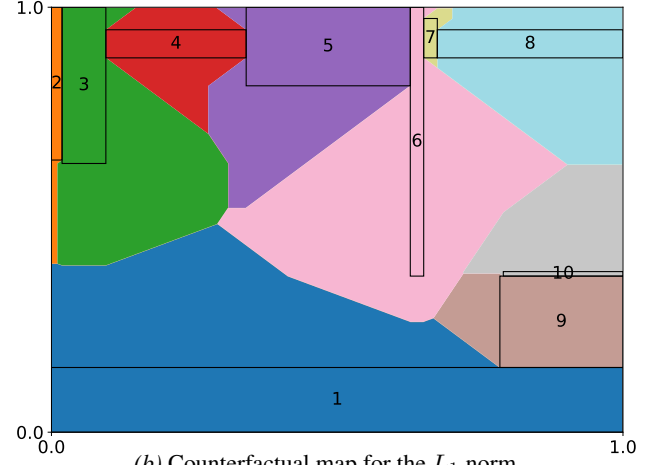
On each $R_s(\mathcal{H})$, $\delta_k(\cdot, \mathcal{H})$ is affine, so $d_2(\cdot, \mathcal{H})^2$ is a quadratic polynomial there. Fix $\mathcal{H}_i, \mathcal{H}_j \in \mathbb{H}_{y'}$ and refine the sign partitions for \mathcal{H}_i and \mathcal{H}_j ; on each resulting polyhedral cell, the bisector condition $d_2(x, \mathcal{H}_i) = d_2(x, \mathcal{H}_j)$ is equivalent to a single quadratic equation, hence $B_{ij}^{(2)}$ is contained in a finite union of quadratic hypersurfaces.

Finally, Voronoi regions are not necessarily polyhedral when $p = 2$. In \mathbb{R}^2 , let $\mathbb{H}_{y'} = \{\mathcal{H}_1, \mathcal{H}_2\}$ with $\mathcal{H}_1 = \{0\} \times [0, 1]$ and $\mathcal{H}_2 = \{(1, 0)\}$ (a degenerate rectangle). On the strip $\{(x_1, x_2) : x_1 \geq 0, 0 \leq x_2 \leq 1\}$, one has $d_2((x_1, x_2), \mathcal{H}_1) = x_1$ and $d_2((x_1, x_2), \mathcal{H}_2) = \sqrt{(x_1 - 1)^2 + x_2^2}$, so the bisector satisfies $x_2^2 = 2x_1 - 1$, a parabola segment. \square

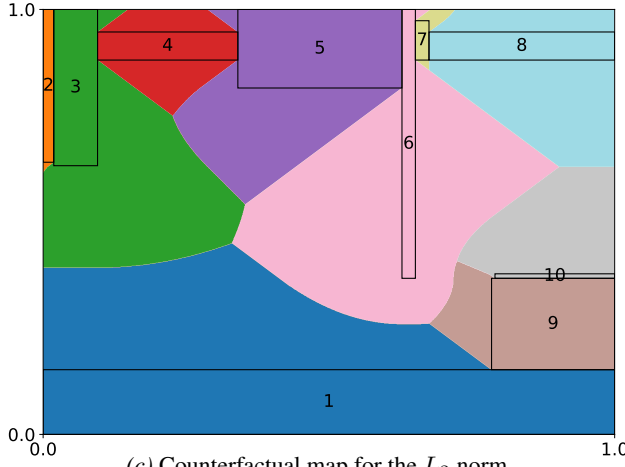
B. Illustrations of Counterfactual Maps under Different Norms



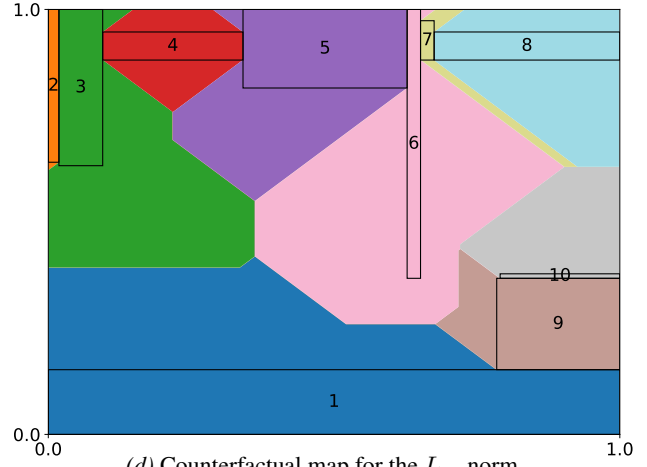
(a) Decision boundaries of the model.



(b) Counterfactual map for the L_1 norm.



(c) Counterfactual map for the L_2 norm.



(d) Counterfactual map for the L_∞ norm.

Figure 7. Counterfactual maps using different norms for target class $[y_2]$. For any input query and distance, the map identifies the closest hyperrectangle of this class; projecting the query onto that region immediately yields a globally optimal counterfactual. This simple two-dimensional example uses a random forest with two depth-5 trees trained on the “blobs” dataset.

C. Proof of Theorem 3.1

C.1. Setting

Fix an integer $m \geq 1$ and a norm index $1 \leq p \leq \infty$. We consider the metric space

$$(\mathbb{R}^m, d_p), \quad d_p(x, x') \triangleq \|x - x'\|_p.$$

Let $\mathbb{H}_{y'} = \{\mathcal{H}_1, \dots, \mathcal{H}_n\}$ be the axis-aligned hyperrectangles associated with target class y' in \mathbb{R}^m , where each

$$\mathcal{H}_i \triangleq [a^{(i)}, b^{(i)}] = \{z \in \mathbb{R}^m : a_k^{(i)} \leq z_k \leq b_k^{(i)} \text{ for all } k = 1, \dots, m\},$$

with $a_k^{(i)} \leq b_k^{(i)}$ for all $k \in \{1, \dots, m\}$.

For any nonempty set $S \subseteq \mathbb{R}^m$ and any $x \in \mathbb{R}^m$, define

$$d_p(x, S) \triangleq \inf_{x' \in S} \|x - x'\|_p.$$

Given a query point $x \in \mathbb{R}^m$, we want to find an index

$$i^* \in \{1, \dots, n\}$$

such that

$$d_p(x, \mathcal{H}_{i^*}) = \min_{1 \leq i \leq n} d_p(x, \mathcal{H}_i).$$

C.2. KD-Tree Structure

We assume a KD-tree construction over $\mathbb{H}_{y'}$ producing a rooted binary tree T whose nodes are denoted by v . For each node v , we associate:

- a nonempty subset of rectangles $\mathbb{H}(v) \subseteq \mathbb{H}_{y'}$ (those stored in the subtree rooted at v);
- an axis-aligned bounding box

$$B(v) \triangleq [\ell(v), u(v)] \subseteq \mathbb{R}^m$$

such that

$$\bigcup_{\mathcal{H} \in \mathbb{H}(v)} \mathcal{H} \subseteq B(v).$$

note that $B(v)$ is defined as the smallest bounding box.

Leaves v satisfy $|\mathbb{H}(v)| \leq k$ (for some fixed k), and we store those rectangles explicitly in the leaf. Internal nodes are built by splitting $\mathbb{H}(v)$ into two disjoint subsets $\mathbb{H}(v_L)$ and $\mathbb{H}(v_R)$ according to some coordinate and threshold (the KD-tree splitting rule).

The construction guarantees the following invariant.

Tree Bounding Box Invariant. For every node v and each child c of v ,

$$\mathbb{H}(c) \subseteq \mathbb{H}(v), \quad \bigcup_{\mathcal{H} \in \mathbb{H}(c)} \mathcal{H} \subseteq B(c) \subseteq B(v).$$

In particular, each child bounding box is contained in the parent bounding box and contains all rectangles in that subtree.

C.3. Query Algorithm

Fix $x \in \mathbb{R}^m$ and define, for each node v of the KD-tree,

$$lb(v) := d_p(x, B(v)).$$

We call $lb(v)$ the *node lower bound*.

The query algorithm `QueryNearest`(x, root, p) is as follows.

- Initialize:

$$d^* \leftarrow +\infty, \quad i^* \leftarrow \text{null}.$$

Let Q be a min-priority queue keyed by $lb(v)$. Insert the root node r with key $lb(r)$.

- While Q is not empty:

1. Extract a node v with smallest key $lb(v)$ from Q .
2. If $lb(v) \geq d^*$, stop the loop.
3. If v is a leaf:
 - For each rectangle $\mathcal{H} \in \mathbb{H}(v)$, compute $d = d_p(x, \mathcal{H})$. If $d < d^*$, then set $d^* \leftarrow d$ and i^* to be the index of \mathcal{H} .
4. If v is an internal node:
 - For each child c of v , compute $lb(c) = d_p(x, B(c))$. If $lb(c) < d^*$, insert c in Q with key $lb(c)$.

At the end, the algorithm returns (i^*, d^*) .

C.4. Lemmas

Lemma C.1 (Distance monotonicity under inclusion). *Let $S, T \subseteq \mathbb{R}^m$ with $S \subseteq T \neq \emptyset$. Then, for all $x \in \mathbb{R}^m$,*

$$d_p(x, T) \leq d_p(x, S).$$

Proof. By definition,

$$d_p(x, T) = \inf_{x' \in T} \|x - x'\|_p.$$

Since $S \subseteq T$, we have

$$\inf_{x' \in T} \|x - x'\|_p \leq \inf_{x' \in S} \|x - x'\|_p,$$

because the infimum is taken over a larger set. Thus $d_p(x, T) \leq d_p(x, S)$. \square

Lemma C.2 (Bounding box as a lower bound). *For any node v and any rectangle $\mathcal{H} \in \mathbb{H}(v)$, we have*

$$lb(v) = d_p(x, B(v)) \leq d_p(x, \mathcal{H}).$$

Proof. By the tree bounding box invariant, $\mathcal{H} \subseteq B(v)$. Applying Lemma C.1 with $S = \mathcal{H}$ and $T = B(v)$ yields

$$d_p(x, B(v)) \leq d_p(x, \mathcal{H}),$$

i.e., $lb(v) \leq d_p(x, \mathcal{H})$. \square

Lemma C.3 (Best-so-far distance over visited rectangles). *At any time during the execution of the algorithm,*

$$d^* = \min\{d_p(x, \mathcal{H}_i) : \mathcal{H}_i \text{ has been explicitly evaluated so far}\},$$

with the convention $\min \emptyset = +\infty$ at initialization.

Proof. Initially, no rectangle has been evaluated and $d^* = +\infty$, so the statement holds.

Whenever the algorithm evaluates a new rectangle $\mathcal{H} \in \mathbb{H}_{y'}$ (this happens only in leaves), it computes its distance $d = d_p(x, \mathcal{H})$. If $d < d^*$, it updates $d^* \leftarrow d$; otherwise d^* remains unchanged. This is exactly the standard maintenance of a running minimum. Therefore, after each update, d^* is the minimum over all rectangles evaluated so far. \square

We now formalize a coverage property for unvisited rectangles.

Lemma C.4 (Coverage invariant). *Call a rectangle visited if its distance has been computed (i.e., it has been iterated over in some leaf). At any iteration of the main loop, every unvisited rectangle \mathcal{H} satisfies at least one of the following:*

- $\mathcal{H} \in \mathbb{H}(v)$ for some node v currently in the priority queue Q ; or
- there exists a node u such that $\mathcal{H} \in \mathbb{H}(u)$ and $lb(u) \geq d^*$, i.e., \mathcal{H} cannot yield a distance strictly smaller than d^* .

Proof. We proceed by induction on the number of iterations of the main loop.

Initialization. At the beginning, no rectangle is visited, and Q contains only the root r . Since $\mathbb{H}(r) = \mathbb{H}_{y'}$, every rectangle belongs to $\mathbb{H}(r)$, and the first condition holds.

Inductive step. Assume the lemma holds at the beginning of an iteration. Let v be the node extracted from Q in that iteration. We consider cases:

- If the algorithm stops immediately because $lb(v) \geq d^*$, then no further iteration occurs, so we are done.
- If v is a leaf: then all rectangles in $\mathbb{H}(v)$ are evaluated in this iteration and thus become visited. Rectangles not in $\mathbb{H}(v)$ are unaffected and remain covered as in the inductive hypothesis. The lemma continues to hold.

- If v is internal: then $\mathbb{H}(v)$ is partitioned into the children subsets, e.g.,

$$\mathbb{H}(v) = \mathbb{H}(v_L) \cup \mathbb{H}(v_R), \quad \mathbb{H}(v_L) \cap \mathbb{H}(v_R) = \emptyset.$$

For each child c , we compute $lb(c)$ and insert c into Q only if $lb(c) < d^*$. Thus any rectangle $\mathcal{H} \in \mathbb{H}(v)$ for which its child c (i.e., child c such that $\mathcal{H} \in \mathbb{H}(c)$) is inserted into Q is covered by a node in Q (the first condition).

If, on the contrary, a child c is not inserted because $lb(c) \geq d^*$, then for any $\mathcal{H} \in \mathbb{H}(c)$, Lemma C.2 gives

$$d_p(x, \mathcal{H}) \geq lb(c) \geq d^*,$$

so such rectangles satisfy the second condition in the statement of this lemma.

Thus, after handling node v , each unvisited rectangle still satisfies one of the two conditions, and the lemma holds for the next iteration (or the algorithm terminates). \square

C.5. Main Optimality Theorem

Theorem C.5 (Exactness of KD-Tree Nearest-Hyperrectangle Search). *Fix $x \in \mathbb{R}^m$ and $1 \leq p \leq \infty$. Run $\text{QueryNearest}(x, \text{root}, p)$ on the KD-tree built over $\mathbb{H}_{y'} = \{\mathcal{H}_1, \dots, \mathcal{H}_n\}$ as described above, and let the algorithm terminate with output (i^*, d^*) . Then*

$$d^* = d_p(x, \mathcal{H}_{i^*}) = \min_{1 \leq i \leq n} d_p(x, \mathcal{H}_i).$$

In other words, the algorithm returns a rectangle whose distance to x is globally minimal among rectangles in $\mathbb{H}_{y'}$.

Proof. By Lemma C.3, at termination we have

$$d^* = \min\{d_p(x, \mathcal{H}_i) : \mathcal{H}_i \text{ has been explicitly evaluated}\}.$$

Thus it suffices to show:

$$\text{No unevaluated rectangle } \mathcal{H} \text{ satisfies } d_p(x, \mathcal{H}) < d^*. \quad (2)$$

Suppose, for contradiction, that there exists an unevaluated rectangle \mathcal{H} with $d_p(x, \mathcal{H}) < d^*$. Consider the iteration in which the algorithm terminates. There are two possible reasons for termination.

Case 1: The queue Q becomes empty.

If Q is empty, there is no node left to process. By Lemma C.4, any unvisited rectangle \mathcal{H} must then fall into the second condition, i.e., there exists a node u such that $\mathcal{H} \in \mathbb{H}(u)$ and $lb(u) \geq d^*$. By Lemma C.2,

$$d_p(x, \mathcal{H}) \geq lb(u) \geq d^*,$$

contradicting $d_p(x, \mathcal{H}) < d^*$.

Case 2: Early stopping when $lb(v) \geq d^$.*

The other termination condition is that the algorithm extracts a node v from Q with minimal key and finds that

$$lb(v) \geq d^*,$$

and thus breaks out of the loop.

Since v has the smallest key in Q , every remaining node $w \in Q$ satisfies

$$lb(w) \geq lb(v) \geq d^*.$$

Let \mathcal{H} be any unvisited rectangle. By Lemma C.4, there exists either a node $w \in Q$ with $\mathcal{H} \in \mathbb{H}(w)$, or a node u with $\mathcal{H} \in \mathbb{H}(u)$ and $lb(u) \geq d^*$. In either case, applying Lemma C.2 yields

$$d_p(x, \mathcal{H}) \geq d^*.$$

Thus no unvisited rectangle can have distance strictly less than d^* , contradicting the hypothesis and proving (2).

Finally, in all possible termination scenarios, every rectangle \mathcal{H} satisfies

$$d_p(x, \mathcal{H}) \geq d^*,$$

and at least one visited rectangle (namely \mathcal{H}_{i^*}) satisfies $d_p(x, \mathcal{H}_{i^*}) = d^*$. Therefore,

$$d^* = \min_{1 \leq i \leq n} d_p(x, \mathcal{H}_i),$$

and the algorithm is exact. \square

D. Additional Experimental Results

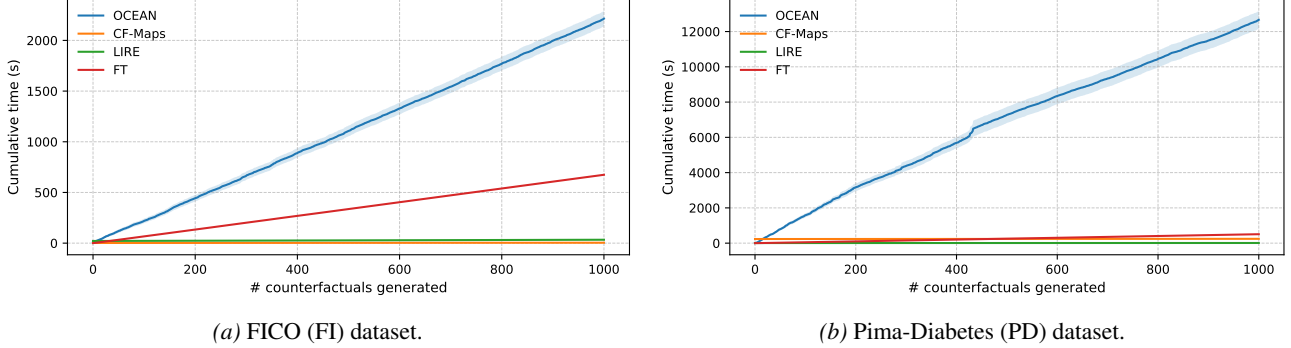


Figure 8. Total runtime (including one-time preprocessing and counterfactual generation) as a function of the number of generated counterfactuals, for random forests with 100 depth-5 trees.

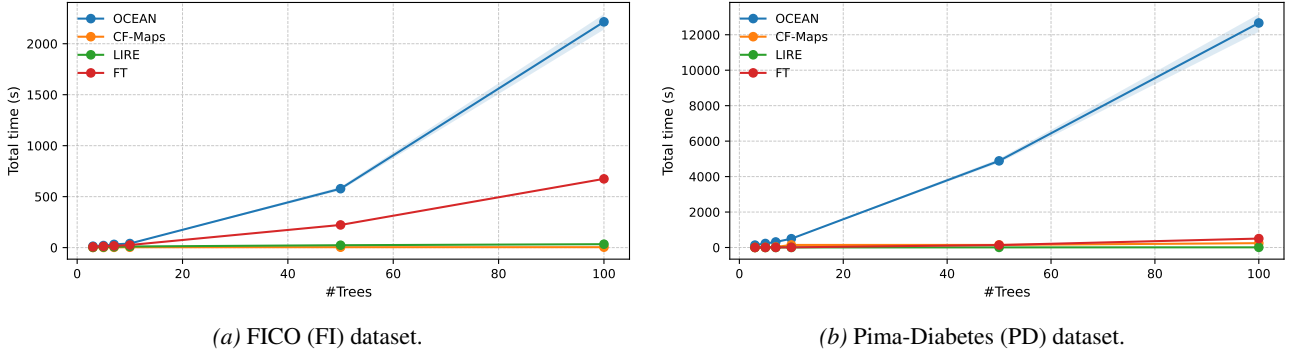


Figure 9. Total runtime (including one-time preprocessing and counterfactual generation) for generating 1000 counterfactuals, for random forests with varying numbers of depth-5 trees.

Table 3. Counterfactual quality of FT and LIRE relative to CF-Maps, for varying numbers of depth-5 trees. The error ratio (R), defined as the ratio between the distance of the returned counterfactual and that of an optimal counterfactual found by CF-Maps or OCEAN, is computed over *valid* counterfactuals only, whereas the failure rate (%Fail) is computed over all explained points.

Dataset	#Trees	FT		LIRE	
		R	%Fail	R	%Fail
Breast-Cancer (BC)	3	1.00	80.2	1.78	0.0
	10	1.00	98.0	1.56	0.0
	50	1.00	93.5	3.07	0.0
	100	1.00	96.0	3.10	0.0
COMPAS (CP)	3	9.17	22.7	1.50	0.0
	10	2.53	49.2	1.38	0.0
	50	2.38	64.5	1.41	0.0
	100	2.00	70.2	1.30	3.0
FICO (FC)	3	5.71	58.8	1.40	0.0
	10	2.74	69.4	1.30	0.0
	50	2.57	77.2	1.29	0.0
	100	1.90	79.9	1.28	0.0
Pima-Diabetes (PD)	3	9.57	87.0	2.39	0.0
	10	4.75	89.7	5.81	0.0
	50	6.21	83.7	7.33	0.0
	100	3.30	82.1	10.21	0.0